HHS Public Access

Author manuscript

Cancer Res Commun. Author manuscript; available in PMC 2023 January 20.

Published in final edited form as:

Cancer Res Commun. 2022 June ; 2(6): 402–416. doi:10.1158/2767-9764.crc-22-0124.

Cancer stem cells, not bulk tumor cells, determine mechanisms of resistance to SMO inhibitors

Joshy George[1,@], **Yaohui Chen**[2,3,@,#], **Nourhan Abdelfattah**[4,@], **Keiko Yamamoto**[5], **Thomas D. Gallup**[6], **Scott I. Adamson**[1,7], **Brad Rybinski**[8], **Anuj Srivastava**[1], **Parveen Kumar**[1], **Min Gyu Lee**[9], **David S. Baskin**[2,3,10], **Wen Jiang**[11], **Jong Min Choi**[12], **William Flavahan**[13], **Jeffrey H. Chuang**[1,8], **Betty YS Kim**[6], **Jiaqiong Xu**[14], **Sung Yun Jung**[15], **Kyuson Yun**[4,16,*]

[1:]The Jackson Laboratory for Genomic Medicine, Farmington, CT, USA

[2:]Department of Neurosurgery, Houston Methodist Neurological Institute and Institute for Academic Medicine, Houston, TX, USA

[3:]The Kenneth R. Peak Brain and Pituitary Tumor Treatment Center, Houston Methodist, Houston TX, USA

[4:]Department of Neurology, Houston Methodist Hospital and Houston Methodist Research Institute, Houston, TX, USA

[5:]The Jackson Laboratory-Mammalian Genetics, Bar Harbor, ME, USA

[6:]Department of Neurosurgery, The University of Texas MD Anderson Cancer Center, Houston, TX, USA

[7:]UConn Health, Department of Genetics and Genome Sciences, Farmington, CT, USA

[8:]Department of Internal Medicine, University of Maryland Medical Center, Baltimore, MD, USA

[9:]Department of Molecular and Cellular Oncology, The University of Texas MD Anderson Cancer Center, Houston, TX, USA

[10:]Department of Neurosurgery, Weill Cornell Medical College, New York, New York

[11:]Department of Radiation Oncology, The University of Texas Southwestern Medical Center, Dallas, TX, USA

[12:]Advanced Technology Core, Mass Spectrometry Proteomics Core, Baylor College of Medicine, Houston, TX, USA

[*]**Corresponding author**: Kyuson Yun, Houston Methodist Research Institute, 6670 Bertner Ave, RI11-116, Houston, TX 77030. Tel: 713-363-9285; kyun@houstonmethodist.org.

[#:]Current address: Department of Thoracic Surgery, West China Hospital, Sichuan University, Chengdu, China.

[@:]These authors contributed equally to this study

AUTHOR CONTRIBUTIONS

KY (PI) conceived and designed the experiments, performed data analyses, and prepared the manuscript. YC, KY, BR, PL, TDG, and SN performed the in vitro and in vivo experiments and analyzed the data. JG, SIA, NA, PK, AN, and JHC analyzed RNAseq and Exome-seq data, and JMC and SYJ generated and analyzed the proteomics data. NA, DSB, MKL, BR, WF, WJ, BYSK, and JHC contributed to data analyses and manuscript preparation. JX and NA performed statistical analyses. All authors contributed to manuscript preparation.

COMPETING INTERESTS:

KY is a co-founder of EMPIRI, Inc.

[13]:Department of Molecular, Cell and Cancer Biology, University of Massachusetts Chan Medical School, Worcester, MA, USA

[14]:Center for Outcomes Research, Houston Methodist Research Institute, Houston TX

[15]:Department of Biochemistry and Molecular Biology, Baylor College of Medicine, Houston, TX, USA

[16]:Department of Neurology, Weill-Cornell Medical College, NY, NY, USA

Abstract

The emergence of treatment resistance significantly reduces the clinical utility of many effective targeted therapies. Although both genetic and epigenetic mechanisms of drug resistance have been reported, whether these mechanisms are stochastically selected in individual tumors or governed by a predictable underlying principle is unknown. Here, we report that the dependence of cancer stem cells (CSCs), not bulk tumor cells, on the targeted pathway determines the molecular mechanism of resistance in individual tumors. Using both spontaneous and transplantable mouse models of sonic hedgehog (SHH) medulloblastoma (MB) treated with an SHH/Smoothened inhibitor, sonidegib/LDE225, we show that genetic-based resistance occurs only in tumors that contain SHH-dependent CSCs (SD-CSCs). In contrast, SHH MBs containing SHH-dependent bulk tumor cells but SHH-independent CSCs (SI-CSCs) acquire resistance through epigenetic reprogramming. Mechanistically, elevated proteasome activity in SMOi-resistant SI-CSC MBs alters the tumor cell maturation trajectory through enhanced degradation of specific epigenetic regulators, including histone acetylation machinery components, resulting in global reductions in H3K9Ac, H3K14Ac, H3K56Ac, H4K5Ac, and H4K8Ac marks and gene expression changes. These results provide new insights into how selective pressure on distinct tumor cell populations contributes to different mechanisms of resistance to targeted therapies. This insight provides a new conceptual framework to understand responses and resistance to SMOis and other targeted therapies.

Keywords

Cancer stem cells; medulloblastoma; SHH inhibitor; LDE225; drug resistance mechanism

INTRODUCTION

The sonic hedgehog (SHH) pathway is a highly conserved developmental signaling pathway that is activated in many human cancers, including basal cell carcinoma (BCC), acute myeloid leukemia (AML), and medulloblastoma (MB) (1,2). Currently, there are two FDA-approved SHH/Smoothened (SMO) inhibitors (SMOis: vismodegib and sonidegib) for treating BCCs and other cancer types in which SHH pathway activity is elevated. Unfortunately, as observed for other highly effective targeted therapies (3), a significant portion of BCC patients initially responsive to SMOis develop resistance over time (4,5,6) or experience tumor rebound upon cessation of treatment (7). In clinical trials for SHH-subtype MBs, an objective response rate of 55% has been reported for sonidegib/LDE225, while vismodegib/GDC-0449 has shown an objective response rate of 17% (8), indicating

that not all SHH-subtype MBs respond to SMOi treatment. A subset of these nonresponders were shown to harbor downstream mutations in the SHH pathway (9), while others developed acquired resistance over time or were inherently nonresponsive (10–16). In BCC patients, most—albeit not all—resistant tumors harbor treatment-induced mutations in SHH pathway components (4,5). However, only approximately 50% of SMOi-resistant MBs were shown to acquire mutations in the SHH pathway in a preclinical study (10), suggesting that additional mechanisms of resistance to SMOis must exist.

MB is a classical developmental cancer (2,17) and is commonly believed to originate from cerebellar granule progenitors (CGPs) that normally depend on SHH signaling for proliferation. More recent studies, however, have shown that SHH MBs can arise from either transformed neural stem cells (NSCs) in the neuroepithelium or CGPs in the external granule layer (EGL) when the SHH pathway is aberrantly activated (18,19). In fact, bulk tumor cells arising from transformed NSCs or CGPs with constitutive *Smoothened* (Smo-M2) expression are indistinguishable. However, cancer stem cells (CSCs) from different cells of origin have distinct cellular characteristics, including their dependence on SHH signaling (18). CSCs retain the epigenetic memory of their cells of origin, including growth factors that they rely on for proliferation and survival. Hence, CSCs that arise from NSCs depend on bFGF and EGF instead of SHH, while CSCs that arise from transformed EGL progenitors depend on SHH signaling (18,20,21). Previously, others have shown that CSCs are more resistant to cytotoxic chemo- and radiotherapies (22,23) and seed tumor recurrence (24,25). However, the role of the differential mitogenic/survival pathway dependencies between bulk tumor cells and CSCs as a potential mechanism of resistance to targeted therapy has not been explored.

Here, we tested our hypothesis that treatment-induced mutations in the targeted pathway (SHH) occur only in tumors in which CSCs depend on the targeted pathway. We hypothesized that in tumors where CSCs and bulk tumor cells depend on different mitogenic pathways, targeted therapy selected based on bulk tumor analysis results in only a transient response (debulking) followed by resistant tumor growth due to the presence of inherently resistant CSCs. Specifically, we tested whether SMOi-resistant tumors containing SHH-dependent CSCs (SD-CSCs) acquire new mutations in the SHH pathway, while SHH MBs containing SHH-independent CSCs (SI-CSCs), i.e., SI-CSC MBs, do not (Fig 1A). The results of this study reveal a novel mechanism of inherent therapeutic resistance and provide a new explanation for the clinical failure of targeted therapies and the emergence of resistant tumors that do not acquire new mutations in the targeted pathway. These findings have significant clinical implications for the selection of targeted therapies, particularly for second-line therapy.

MATERIALS AND METHODS

Mouse models and in vivo drug treatment:

Ptch (*Ptch1*^{tm1Mps}/J IMSR Cat# JAX:003081, RRID:IMSR_JAX:003081), *FSmoM2* (Gt (ROSA)26Sor<tm1 (Smo/EYFP)Amc>/J, IMSR Cat# JAX:005130, RRID:IMSR_JAX:005130), h*GFAP-cre* (FVB-Tg(GFAP-cre)25Mes/J, IMSR Cat# JAX:004600, RRID:IMSR_JAX:004600), *p53* (B6.129S2-*Trp53*^{tm1Tyjl}/J, IMSR Cat#

JAX:002101, RRID:IMSR_JAX:002101), NSG (NOD. Cg-*Prkdc*^{scid} *Il2rg*^{tm1Wjl}/SzJ (IMSR Cat# JAX:005557, RRID:IMSR_JAX:005557) and B6 (C57BL/6J, IMSR Cat# JAX:000664, RRID:IMSR_JAX:000664) mice were obtained from the JAX repository. MB subtype determination was performed as previously described[23]. To eliminate potential spatial heterogeneity within the parental tumor, each *Ptch;p53* spontaneous MB was first minced into a slurry, and equivalent pools of tumor cells were injected into male or female 6- to 8-week-old NSG mice. When the tumor volume reached 100–200 mm^3, mice were treated with 40 mg/kg LDE225 or vehicle control (oral gavage, every three days) until harvest. *FSmoM2;hGFAP-cre* pups were treated with LDE225 using the same dose and schedule as *Ptch;p53* MBs, starting at p2 or p3. Mice were randomly assigned to each group and were age- and sex-matched at the time of the experiment. Mice were housed and handled in accordance with the protocols and procedures approved by The Jackson Laboratory and the HMRI Institutional Animal Care and Usage Committees (IACUC).

Tumor subtype characterization:

The SD-CSC and SI-CSC tumor subtype designation methods were previously reported (18). Briefly, freshly dissociated single cells were isolated from spontaneous MBs and plated at a low density (3000 cells in 3 ml) in either TSC (modified DME/F-12 supplemented with B27 (Invitrogen) and penicillin/streptomycin) or NSC (TSC plus 20 ng/ml EGF and 10 ng/ml bFGF) medium in triplicates in 6-well plates, and secondary sphere formation was scored 5–7 days later. Tumors that formed secondary spheres only in NSC but not TSC medium were designated growth-factor-dependent (GFD)/SI-CSC subtype. Those that formed spheres in either NSC or TSC medium were designated as growth-factor-independent (GFI)/SD-CSC subtype. Those that did not form secondary spheres in either TSC or NSC medium were designated as no growth (NG)/SD-CSC subtype based on additional analyses (18).

Primary cells and in vitro drug treatment:

Primary tumorsphere cells were isolated from *Ptch;p53* or *FsmoM2;hGFAP-Cre* mouse MBs and cultured in serum-free, neural stem cell medium with or without exogenous growth factors, bFGF and EGF. For SD-CSC tumor cells, we used NSC medium. SI-CSC tumorspheres were cultured in the TSC medium. Cells were treated with the indicated concentrations of inhibitors: LDE225 (10 μM, cat # 500511 from Chemie Tek), GANT61 (10 μM, cat# 3191 from TOCRIS Bioscience), and trichostatin A (0.01 μM or 0.1 μM, cat# T8552 from SIGMA). Histone acetyltransferase inhibitor IV (10 μM, cat# 382111 from EMD Millipore Corp.), histone acetyltransferase inhibitor VIII (10 μM, cat# 382111 from Calbiochem), MG132 (25 μM, cat# M7449 from Sigma) and JQ1 (0.01 μM or 0.1 μM, provided by J. Bradner).

No established cell lines were used in this study. Cells used in this study were freshly dissociated spontaneous mouse tumors that developed in our animal facility. Mice that develop spontaneous tumors are genotyped in our lab using PCR assays before tumor harvests. Additionally, our lab routinely tests for potential mycoplasma infection by a PCR assay to ensure that all cultured cells are mycoplasma-free. Cryo-preserved primary cells used in the study were tested negative for Mycoplasma upon recovery.

Whole exome sequencing analysis:

Raw fastq reads from bulk exome sequencing data were mapped to the mouse reference genome GRCm38 using BWA, RRID:SCR_010910 (version 0.7.12)(26),), followed by removal of duplicate reads using Picard, RRID:SCR_006525 (version 2.1) (http://broadinstitute.github.io/picard/). The resulting BAM files were further realigned around indels and recalibrated for base quality using GATK, RRID:SCR_001876 (version 3.5.0)(27). For GATK, the known variant sites were downloaded from the Wellcome Trust Sanger Institute, v5 release REL-1505-SNPs_Indels (ftp://ftp-mouse.sanger.ac.uk/REL-1505-SNPs_Indels). Next, the recalibrated BAM files were used as tumor-normal pairs to detect somatic mutations using MuTect, RRID:SCR_000559. Finally, SnpEff, RRID:SCR_005191(28) was used to annotate the somatic mutations, and only the variants annotated as high impact and showing no mutant reads in the normal sample were used for downstream analysis. The copy number analysis for bulk exome datasets was performed using the Sequenza algorithm with default parameters. Only the copy number segments greater than 1 MB in size were used for downstream analysis.

RNA-seq analysis:

RNA-seq analysis was carried out using the in-house pipeline at The Jackson Laboratory. Trimmomatic, RRID:SCR_011848 (version 0.33) was used to remove adapters and leading and trailing low-quality bases. Reads fewer than 36 bases long were discarded. Reads with more than 50% low-quality bases overall were filtered out, and the remaining high-quality reads were then used for expression estimation. Alignment estimation of gene expression levels using the EM algorithm for paired end read data was performed using RSEM, RRID:SCR_013027 (package version 1.2.12). RSEM uses Bowtie 2 and RRID:SCR_016368 as aligners to align the mapped reads against the mm10 reference genome. Data quality control was performed using Picard, RRID:SCR_006525 (version 1.95) (http://broadinstitute.github.io/picard/) and Bamtools, RRID:SCR_015987 to obtain general alignment statistics from the bam file. Analyses of aligned reads were performed using the R package edgeR, RRID:SCR_012802. Gene set enrichment pathway analysis was performed using edgeR preranked gene lists with the fgsea (fgsea, RRID:SCR_020938) and GAGE (RRID:SCR_017067) R packages or log2 normalized CPM values with the gene set visualization analysis (GSVA) R package. Plots were generated using ggplot2 and RRID:SCR_014601, and heatmaps were generated using ComplexHeatmap and RRID:SCR_017270.

Proteomics analysis:

Label-free proteome profiling was carried out as previously described(29). Briefly, the cell pellets were dissolved in 50 mM ammonium bicarbonate and 1 mM CaCl2 buffer followed by 3 rounds of liquid nitrogen freezing and 95°C boiling for 2 min. The lysate was digested by trypsin (Gendepot T9600) at 37°C overnight. The tryptic peptides were desalted prefractionated into 5 fractions using C18 beads. LC–MS/MS analysis was carried out using a nanoLC1200 system coupled to an Orbitrap Fusion™ Tribrid™ mass spectrometer (Thermo Fisher Scientific, San Jose, CA). One microgram of peptide was loaded onto a C18 (1.9 μm, Reprosil-Pur Basic Dr. Maisch GmbH, Germany) trap

column and switched in-line with a 50 mm x 150 μm analytical column packed with the same C18 beads. The peptides were eluted using a 75 min linear gradient of 4% to 26% acetonitrile, ionized, and measured in data-dependent mode acquiring fragmentation spectra of the top 30 strongest ions and under the direct control of Xcalibur software ver. 4.0 (Thermo Xcalibur, RRID:SCR_014593). The MASCOT search engine (Mascot, RRID:SCR_014322) was used to match the spectrum to the corresponding peptide sequence searched against NCBI's mouse RefSeq protein. The Mascot results were validated with the Percolator-based q-value in the Proteome Discoverer software (ThermoFisher, PD2.1-(RRID:SCR_014477)). Dynamic modification was allowed for oxidation (methionine), protein N-terminal acetylation, and deamidation (asparagine and glutamine). The maximum tolerance for precursor ions was set to 20 ppm; the fragment mass tolerance was set to 0.5 daltons; and a maximum of two missed cleavages was allowed. The calculated area under the curve of peptides was used to calculate iBAQ and iFOT for protein abundance based on a previous publication(29).

Bisulfite sequencing analysis:

Raw bisulfite sequencing reads were aligned using bismark (v0.23.1) (RRID:SCR_005604) (30) and bowtie2 (v2.4.4)(31) (RRID:SCR_016368) onto the reference mouse genome Grcm38. Subsequently, the duplicate reads that aligned to the same position and in the same orientation were removed using "deduplicate_bismark" from the bismark bisulfite mapper. Methyl seq data were further analyzed by fusing the methylKit R-package from Bioconductor(32). Principal component analysis (PCA) was performed to generate a low-dimensional representation of methylation profiles using the method available from the same package.

Gene set enrichment pathway analysis:

GSEA was performed using msmsTests::msms.edgeR() preranked gene lists with fgsea (fgsea, RRID:SCR_020938), GAGE (RRID:SCR_017067) R packages or log2 normalized iFOT values with gene set visualization analysis (GSVA) R package. Plots were generated using ggplot2 (RRID:SCR_014601), and heatmaps were generated using ComplexHeatmap (RRID:SCR_017270).

Proteasome reporter assay:

Cell-Based Proteasome-Glo Assay for Chymotrypsin-like protease activities (Promega) was performed following the manufacturer's instructions. Equal numbers of cells were plated, and the reporter assay levels were normalized to viability in each sample. All assays were repeated at least three times in triplicate, and error bars represent the SEM.

Survival analysis of the external human medulloblastoma dataset:

To assess the correlation between BRD2 or BRD4 expression and survival in the publicly available human medulloblastoma dataset (Cavalli dataset: GSE85217) (33), Kaplan–Meier survival analysis was performed by stratifying patients based on median expression using the "survival" R package (https://github.com/therneau/survival) and plotted using the "survminer" R package (https://github.com/kassambara/survminer)

Immunoblot analysis:

Total proteins from tissue or cells were obtained using RIPA buffer supplemented with protease and phosphatase inhibitor cocktails. A total of 30–50 μg of lysates was resolved on 10% or 15% SDS–PAGE gels, and proteins were transferred to PVDF membranes (BioRad, cat # 162–0177). Subsequent western analyses were performed using standard procedures. Antibodies against CBP (RRID: AB_2616020, 1:1000), GCN5 (RRID: AB_2128281, 1:3000), PCAF (RRID: AB_2128409, 1:3000), HDAC1 (RRID: AB_10612242, 1:2000), HDAC2 (RRID: AB_10624871, 1:3000), HDAC3 (RRID: AB_2118371, 1:3000), histone H3 (RRID: AB_10544537, 1:10000), H3K9ac (RRID: AB_823528, 1:50000), H3K14ac (RRID: AB_10839410, 1:5000), H3K18ac (RRID: AB_2783723, 1:30000), H3K27ac (RRID: AB_10949503, 1:15000), H3K56ac (RRID: AB_10548193, 1:1000), histone H4 (RRID: AB_1147658, 1:1000), H4K5ac (RRID: AB_11217428, 1:100000), H4 Antibodies against Gli1 (sc-515751, 1:1000), actin (RRID: AB_2223345, 1:3000) and tubulin (RRID: AB_1130901, 1:3000) were purchased from Santa Cruz. Antibodies against HAT1 (RRID: AB_2116435, 1:3000) were purchased from Proteintech. For *Ptch;p53* SD-CSC tumors shown in figure 2, 4, and 5, same *ß-ACTIN loading control image is shown since same samples were loaded on multiple gels on the same day and membranes were cut into multiple pieces to probe different proteins shown.

Immunohistochemistry:

Immunohistochemistry was performed following standard protocols using paraffin sections with the indicated primary antibodies: NEUN (Millipore, RRID: AB_2298772, 1:200).

Statistical analyses:

Statistical comparisons were performed using GraphPad Prism (RRID:SCR_002798) or R Project for Statistical Computing (RRID:SCR_001905). Values and error bars represent the mean ± standard error of the mean (SEM). The respective number of replicates (n) values are indicated in figures or in figure legends. P values were determined by an appropriate statistical test, such as Student's t-tests or analysis of variance (ANOVA), with multiple comparison corrections, as indicated in the figure legend. Fisher's exact test was used to test the difference in the rate of acquired mutations in the different subtypes.

Data availability:

Exome-seq and methyl-seq data are available through the SRA portal (https://www.ncbi.nlm.nih.gov/bioproject/PRJNA793810). RNA-seq data are available through the SRA portal (https://www.ncbi.nlm.nih.gov/bioproject/PRJNA834841).

The publicly available human gene expression profiling dataset GSE85217 (https://www.ncbi.nlm.nih.gov/geo/query/acc.cgi?acc=GSE85217) was downloaded from GEO and used to analyze BRD2 and BRD4 expression levels in different MB subtypes and survival(33). The proteome profiling data have been deposited to the MASSIVE repository (MSV000087151).

RESULTS

Acquired mutations in the SHH pathway occur only if CSCs depend on the SHH pathway

To experimentally test our hypothesis that the dependence of CSCs, rather than bulk tumor cells, to the targeted pathway determines the molecular mechanism of therapeutic resistance (Fig 1A), we first used an autochthonous SHH MB mouse model (*FSmoM2;hGFAP-cre*) in which the activated SMO (SMO-M2) allele is conditionally expressed upon Cre recombinase expression(34). We previously reported that 100% of *FSmoM2;hGFAP-cre* mice develop MBs and hydrocephalus and die around weaning age (18). Furthermore, all MBs that arise from transformed NSCs in *FSmoM2;hGFAP-cre* are SI-CSC tumors, due to Cre expression in the neuroepithelium (35). CSCs in *FSmoM2;hGFAP-cre* MBs depend on bFGF/EGF and not SHH, similar to their cell of origin (NSCs), and they are insensitive to SHH inhibition (18), even though the SHH pathway is highly activated in bulk tumor cells in this model (Supp Fig 1A). When *FSmoM2;hGFAP-cre pups were treated with* LDE225, we observed milder hydrocephalus and consistently smaller brains in the treated mice (Fig 1B). However, SMOi treatment alone was not sufficient to significantly increase survival in *FSmoM2;hGFAP-cre* mice (Fig 1C), even though LDE225 treatment had the intended on-target effect of reducing SHH pathway activity in vivo, as demonstrated by the lower GLI1 expression level in treated mice (Fig 1D).

To validate our findings in an independent model, we performed the same experiment in a well-characterized transplantable model of *Ptch;p53* SHH MB (18). In this model, *Ptch* and *p53* mutations are germline, and cellular transformation can occur in either NSCs or CGPs in different mice, resulting in either SI-CSC or SD-CSC MBs, respectively (18). We isolated primary tumorspheres from spontaneous *Ptch;p53* MBs and characterized each MB as either the SD-CSC or SI-CSC subtype by in vitro culture phenotypes (Supp Table 1, (18)). In addition, we performed whole-genome bisulfite sequencing analysis to test their epigenomic differences and observed that SD-CSCs clustered together but away from SI-CSCs (Supp Fig 1B, Supp Table 2). In parallel, we injected primary, uncultured tumorspheres from three independent *Ptch;p53* MBs into *NOD-SCID;Il2gr$^{-/-}$ (NSG)* host mice to generate three allograft cohorts with isogenic tumors (Supp Fig 1C). When the tumor volume was ~100 mm^3, we divided each cohort into two groups, treated the mice with either vehicle or LDE225, and measured tumor growth. All mice initially responded to LDE225 treatment, and the tumor volume was reduced 3–4 days after the first treatment (Supp Fig 1D). When the tumor volume had decreased to <50 mm^3, we halted treatment and evaluated the mice for tumor recurrence. When the tumors rebounded (to >100 mm^3), we resumed treatment. In all SI-CSC MBs, resistant tumors grew immediately after the initial debulking phase (Supp Fig 1D). In contrast, in most SD-CSC MBs, multiple rounds of SMOi treatment were required for the emergence of resistant tumors, suggesting that they required acquisition of additional mutations (Supp Fig 1D). Consistently, mice bearing *Ptch;p53* SD-CSC intracranial tumors tended to survive longer than vehicle-treated mice, but this difference did not reach statistical significance (p= 0.1591, Supp Fig 1E).

Next, we analyzed each resistant tumor for treatment-induced mutation through whole-exome sequencing (coverage >120X) from both *Ptch;p53* and *FSmoM2;hGFAP-cre* MBs.

To account for baseline mutational profile differences in each spontaneous *Ptch;p53* tumor, we compared control- and SMOi-treated MBs from each cohort separately. Compared to control-treated MBs within each cohort, SMOi-treated tumors exhibited 14 to 146 new SNPs with allele frequency changes >20% (Supp Fig 1F, Supp Tables 4, 5). As anticipated, acquired mutations in SHH pathway genes were detected in SMOi-resistant *Ptch;p53* SD-CSC tumors (4 of the 6 tested, 66.7%; Fig 1F, G, H, Supp Fig 1G, Supp Table 3). These mutations included a mutation in the *Smo* gene, SmoL416F, which corresponds to the L412F mutation in humans (Fig 1G); *Gli2* amplification (Fig 1H); and Mycn amplification (Fig 1F). These SHH pathway mutations have been previously reported in SMOi-resistant MBs and BCCs (5,10,11). In contrast, none of the *Ptch;p53* SI-CSC SMOi-resistant tumors had mutations in the SHH pathway (0 of 3 *Ptch;p53* MBs, Supp Table 4). Histologically, control MBs were indistinguishable from LDE225-resistant *Ptch;p53* MBs of both the SI-CSC and SD-CSC subtypes (Supp Fig 1H).

To validate this finding in an independent model, we performed additional WES from seven *FSmoM2;hGFAP-cre* MBs. Remarkably, none of the seven LDE225-treated *FSmoM2;hGFAP-cre* MBs had acquired mutations in the SHH pathway (Fig 1E, Supp Fig 1I, Supp Table 5). Together, drug-induced mutations in the SHH pathway were observed in 4 of 6 vs. 0 of 10 (66.67% vs. 0%, p=0.008) SHH MBs in the SD-CSC vs. SI-CSC subtypes, respectively. These results in two different SHH MB models strongly support our hypothesis that treatment-induced mutations in the SHH pathway occur only when the CSCs depend on the SHH pathway.

SMOi-treated SI-CSC MBs bypass the SHH pathway

To confirm that LDE225 treatment suppresses the SHH pathway in both SI-CSC and SD-CSC *Ptch;p53* MBs, we performed RT–PCR on tumors subjected to both acute and long-term treatment. Acute treatment (3 days in vivo) in both subtypes resulted in significant reductions in the levels of SHH pathway genes (Supp Fig 2A), indicating that on-target, therapeutic dosing of LDE225 was achieved in both tumor subtypes. Upon long-term treatment with LDE225, the RNA levels of the known SHH pathway genes *Ptch1, Smo, Gli1,* and *Gli2* were equivalent to those in control-treated tumors in SD-CSC MBs (Fig 2A), indicating continued activation of the SHH pathway consistent with acquired mutations in this pathway. One of the SD-CSC tumors with *Gli2* amplification had a higher expression level of *Gli2*. In contrast, in SMOi-resistant *Ptch;p53* SI-CSC tumors, *Gli1* RNA and protein levels were significantly reduced (Fig 2A, B). These observations strongly suggest that SI-CSC MBs acquire resistance to SMOis through an alternative mechanism that bypasses the need for SHH pathway activation.

To functionally test this hypothesis, we treated control and SMOi-resistant *Ptch;p53* SI-CSC and SD-CSC tumorspheres with GANT61, a small molecule inhibitor of GLI1 (36). Others have shown that SMOi-resistant tumors may be inhibited by targeting the downstream effector of the SHH pathway, GLI1(37). Previously, we reported that *Ptch;p53* SD-CSC tumorspheres but not SI-CSC tumorspheres are sensitive to LDE225 in vitro (18). As anticipated, both control and LDE225-resistant *Ptch;p53* SD-CSC tumorspheres were sensitive to GLI1 inhibition, confirming their continued dependence on the SHH

pathway (Fig 2C). In contrast, control and SMOi-resistant *Ptch;p53* SI-CSC tumorspheres were insensitive to GLI1 inhibition (Fig 2C), confirming their independence from the SHH pathway.

SI-CSC MB progenitors follow an alternative differentiation trajectory upon SMOi treatment

To conduct an unbiased investigation of the mechanism by which SI-CSC MBs continue to grow in the presence of SMOis, we performed RNA-seq analyses of matched control- and LDE225-treated *FSmoM2;hGFAP-cre* SI-CSC MBs (Supp Fig 2B, Supp Table 6). A total of 893 genes were significantly differentially expressed (DE) (false discovery rate (FDR)<0.05, log fold change (FC)>1, Supp Table 6). These changes included downregulation of the SHH pathway targets *Gli1, Ccnd1*, and *Myc*; downregulation of the NSC marker genes *Nestin* and *Sox2*; downregulation of the Notch pathway genes *Hes1, Hes5, and Jag1*; downregulation of the cerebellar granule neuronal progenitor marker *Atoh1*; upregulation of cerebellar neuronal differentiation markers *NeuroD1* and *Zic1*; and other alterations (Fig 2D, Supp Fig 2C,D). Collectively, these changes suggested increased neuronal differentiation in LDE225-treated tumors. Consistent with these findings, pathway analyses of differentially expressed genes by gene set enrichment analysis (GSEA), gene set variation analysis (GSVA), and Ingenuity Pathway Analysis (IPA) showed consistent enrichment of pathways associated with increased neuronal differentiation, reduced proliferation, and reduced Hedgehog signaling (Fig 2E). Immunohistochemical analyses comparing vehicle- and LDE225-treated tumors confirmed significantly increased NeuN expression in LDE225-treated tumors (Fig 2F). Together, these results indicated that SHH pathway activation in *FSmoM2;hGFAP-cre* mice transforms NSCs by maintaining them in a more NSC/early EGL progenitor-like state marked by high *Sox2, Nes,* and *Atoh1* expression and blocking their terminal differentiation into neurons. However, LDE225 treatment enhanced differentiation, resulting in decreased *Sox2, Sox1, Nes,* and *Atoh1* expression and increased *NeuroD1, Zic1* and NEUN expression (Fig 2D, F). Note that the expression levels of receptors for NSC growth factors EGF and bFGF were not significantly altered, while *Ptch1* and *Smo* expression was reduced (Fig 2D). RNA-sequencing analysis of *Ptch;p53* SI-CSCs showed the same general trend, with significantly reduced *Gli1* expression in SI-CSC tumors but not in SD-CSC tumors (Supp Fig 2E, Supp Table 7 & 8).

Epigenetic reprogramming in SMOi-resistant SI-CSC MBs—Other investigators have also reported the emergence of LDE225-resistant *Ptch;p53* MBs that do not acquire mutations in the SHH pathway (10), but the mechanism underlying these resistant tumors is not well understood. Hence, we next focused on elucidating the mechanism underlying SMOi resistance in the absence of activating mutations in the SHH pathway. We hypothesized that SI-CSC MBs continue to grow in the presence of LDE225 by bypassing the SHH-dependent CGP-like cell state through epigenetic reprogramming of bulk tumor cells (Fig 1A). To test this hypothesis, we performed targeted pathway analyses of differentially expressed genes identified by RNA-seq in vehicle- vs. LDE225-treated *FSmoM2;hGFAP-cre* MBs. Multiple pathways associated with histone acetylation and methylation were significantly enriched (normalized enrichment score (NES)>2, Fig 3A, Supp Fig 2F), suggesting significant epigenetic reprogramming in LDE225-treated tumors. Since the role of differential histone methylation during development and drug resistance

is well established (38,39), we focused our analysis on histone acetylation changes. The RNA-seq results from *Fsmo;hGFAP-Cre* MBs showed significant downregulation of histone acetyltransferases (HATs: *Hat1* and *Kat2a/GCN5*), the histone deacetylase (HDAC) *Hdac1*, and the histone acetylation reader *Brd2* between vehicle and LDE treated samples (Fig 3B, C, Supp Fig 2F, G, H). Interestingly, the *Kat2b/PCAF, HDAC5, 7, and 11* RNA levels were increased in resistant tumors, and the RNA level of *Brd4*, previously reported to mediate SMOi resistance in SHH MBs by upregulating *Gli1* expression (40), was not significantly altered (Fig 3B, C). To determine whether the changes in these epigenetic regulator expression patterns are generic responses to LDE225 in all MBs, we also analyzed *Ptch;p53* SI-CSC and SD-CSC MBs treated with LDE225 by RNA-seq. While SI-CSC *Ptch;p53* MB samples exhibited differential expression of the genes in histone acetylation and methylation pathways in LDE225-treated tumors, there was no significant difference between vehicle- and LDE-resistant SD-CSC MBs (Fig 3D), suggesting that these processes are not generic responses to SMOi treatment in all MB subtypes; rather, they are specifically associated with SI-CSC tumors.

To independently test whether similar epigenetic changes are observed at the protein level, we performed a proteomics analysis of *Ptch;p53* SI-CSCs and SD-CSCs treated with LDE225 (Supp Fig 3A, B, C). A total of 7540 gene protein products (GPs) were recovered from 5 control and 4 LDE225-treated samples by mass spectrometry-based label-free proteome profiling. We identified 244 GPs that were significantly upregulated and 203 GPs that were significantly downregulated in SMOi-resistant tumors by LDE225 treatment (Supp Table 9). Pathway analyses showed significant upregulation of proteins associated with macromolecule degradation and metabolism of amino acids, lipids, and glucose; downregulation of DNA repair pathways/cell cycle progression; and other alterations (Supp Fig 3D). Consistent with the RNA-seq results, biological process gene sets associated with histone acetylation, methylation, and phosphorylation were enriched with differentially expressed proteins in LDE225-resistant SI-CSC samples (Fig 3E, Supp Fig 3E). In addition, ATOH1, GLI2, and SOX1 protein levels were significantly reduced in SI-CSC MBs but not in SD-CSC MBs that were resistant to LDE225 (Supp Fig 3F). The HAT1 protein level was reduced, although not significantly ($p>0.05$); however, HDAC1 and BRD4 levels were significantly downregulated at the protein level (Fig 3F), suggesting potential posttranscriptional regulation of the protein expression of some genes.

Since *Brd2* and *Brd4* expression was reduced in LDE225-treated *Ptch;p53* MBs at either the RNA or protein level, we analyzed the expression levels and prognostic value of Brd2/4 in a published gene expression and survival dataset of human MB (33). Although the *BRD4* level did not stratify patient survival in the total MB cohort (Supp Fig 4A), a lower *BRD4* expression level was associated with significantly better survival in the SHH MB subgroup (Fig 3G). While lower *BRD2* expression predicted better survival in the total MB cohort, lower *BRD2* expression was not significantly associated with better survival in the SHH subgroup (Fig 3G, Supp Fig 4B).

Altered histone code in LDE225-resistant SI-CSC MBs

Our high-throughput analyses at the RNA and protein levels showed consistent alterations in histone modification pathways in LDE225-resistant SI-CSC MBs in both the *FSmoM2;hGFAP-cre* and *Ptch;p53* models. To determine the functional consequences of these alterations, we first examined the expression levels of HATs (i.e., writers) and HDACs (i.e., erasers) in an independent cohort of samples by Western blot analysis of both MB models. We observed a dramatic reduction in the protein levels of specific HATs (HAT1, CBP, and GCN5 but not PCAF) in SMOi-resistant *FSmoM2;hGFAP-cre* and *Ptch;p53* SI-CSC tumors compared to vehicle-treated tumors. (Fig 4A, B). This was not a general reduction in all HAT proteins, since the PCAF protein level was unchanged or slightly increased, consistent with the RNA-seq analysis results (Fig 4A, B). In contrast, there was no significant change in these HAT protein levels in *Ptch;p53* SD-CSC tumors in vivo (Fig 4C). HDAC1 and HDAC2 levels did not differ consistently between the two models, but the HDAC3 protein level was consistently reduced in both SI-CSC MB models (Fig 4D, E). Again, these changes in HDAC levels were not observed in *Ptch;p53* SD-CSC MBs (Fig 4F). Notably, these changes in the histone machinery in SI-CSC MBs were reproducible in vitro in long-term LDE225-treated *Ptch;p53* and *FSmoM2;hGFAP-cre* primary MB tumorspheres (Fig 4G), indicating a generalizable epigenetic mechanism that occurs both in vivo and in vitro. Notably, this response was not an acute response to SMOi treatment, since short-term (up to 24 hours) LDE225 treatment did not reduce the protein levels of HATs or HDACs (Fig 4H), indicating that these changes are adaptative mechanisms to chronic SMOi exposure and likely contribute to deviations from generating SHH-dependent CGPs in LDE225-resistant SI-CSC MBs. Together, these observations demonstrated that the downregulation of specific histone acetylation regulators in response to chronic SMOi exposure is a robust mechanism that is readily reproducible in multiple experimental systems in vivo and in vitro.

Altered histone code and synthetic lethality with an HDAC inhibitor in SI-CSC MBs—To elucidate the functional outcomes of altered HAT and HDAC protein levels, we analyzed histone marks regulated by HAT1, GCN5, and CBP (41–43). H3K9Ac, H3K14Ac, H3K56Ac, H4K5Ac, and H4K8Ac marks were significantly reduced in both *FSmoM2;hGFAP-cre* and *Ptch;p53* SI-CSC MB mouse models treated with LDE225 (Fig 5A, B). In contrast, H3K27Ac and H4K12Ac levels, which are regulated by other HATs, were not consistently affected (Fig 5A, B), indicating specific rather than global downregulation of histone acetylation in SMOi-resistant tumors. Furthermore, these histone acetylation changes were reproducible in vitro in *FSmoM2;hGFAP-cre* and *Ptch;p53* primary MB tumorspheres subjected to long-term treatment with LDE225 (Fig 5C, D). Importantly, these changes were not observed in *Ptch;p53* SD-CSC tumors (Fig 5E), which acquire genetically driven resistance to LDE225 through continued activation of the SHH pathway.

Finally, to determine whether the observed dysregulation of the histone acetylation machinery offers an opportunity for synthetic lethality, we treated control and SMOi-resistant isogenic *Ptch;p53* SI-CSC tumorsphere cells with HAT, HDAC, and BET protein inhibitors in vitro. Targeting different HAT family members with HATi IV and HATi VIII

did not affect the proliferation/survival of either control or SMOi-resistant cells (Supp Fig 5A, B). In contrast, treatment with an HDAC inhibitor, TSA (10 nM), significantly reduced the viability of SMOi-resistant SI-CSC cells but did not affect isogenic vehicle-treated cells (Fig 5F), indicating that reduced histone acetylation is critical to the survival of LDE225-treated SI-CSC MB cells in vitro.

Considering the clinical interest in BET domain inhibitors for treating MBs (44,45), we also tested whether SMOi-resistant *Ptch;p53* SI-CSC MBs remain sensitive to JQ1, a small molecule inhibitor of BRD4 and other BET domain proteins. Interestingly, JQ1 significantly reduced the viability of both control and SMOi-resistant SI-CSC tumorspheres (Fig 5G), suggesting that SMOi-resistant SI-CSC MBs remain sensitive to BET inhibition. This observation suggests additional mechanisms of action for JQ1 in addition to the regulation of *Gli1* transcription, as previously reported (40).

Increased proteasome activity and degradation of specific HATs

Since the RNA and protein expression levels of the histone regulatory components Brd2, Brd4, GCN5, and CBP were inconsistent between the RNA-seq and proteomics analysis data (Fig 3C, Supp Fig 2H, Fig 4B, E, and Fig 6A, B), we hypothesized that a posttranscriptional mechanism may regulate selective histone regulator protein levels. Consistent with this hypothesis, we observed that the KEGG “proteasome pathway” was a significantly enriched pathway in LDE225-treated MBs (Fig 6C). We first measured the half-life of HAT proteins in control and SMOi-resistant *Ptch;p53* SI-CSC tumorspheres. In control cells, the half-life of CBP and GCN5 was > 8 hours (Fig 6D). In contrast, the half-life of CBP and GCN5 was ~2 hours in SMOi-resistant cells, suggesting that the degradation of CBP and GCN5 was significantly enhanced in LDE225-resistant cells. To determine whether this enhancement was due to the elevated proteasome activity in LDE225-treated cells, we performed a proteasome activity assay and observed that SMOi-treated *Ptch;p53* SI-CSCs had significantly increased proteasome activity compared to control isogenic cells (>2.6-fold, $P<0.0001$, Fig 6E). Consistent with this finding, inhibiting the proteasome with MG132 restored GCN5 and CBP protein levels in LDE225-treated SI-CSCs (Fig 6F). Notably, acute treatment of naïve SI-CSC tumorspheres with LDE225 for 24 hours did not alter the protein levels of CBP and GCN5 (Fig 6G), indicating that this phenotype is not a direct effect of the drug but rather an adaptive mechanism activated upon chronic exposure to SMOis. Together, these results suggest that *Ptch;p53* SI-CSC MB cells epigenetically reprogram bulk tumor cells upon chronic SMOi exposure by elevating proteasome activity to degrade specific HATs, consequently changing the histone code and gene expression in SMOi-resistant SI-CSC tumors (Fig 6H).

DISCUSSION

This study advances our understanding of targeted therapy resistance mechanisms in three significant ways. First, we provide evidence that whether a tumor acquires new mutations (a genetic mechanism) in the targeted pathway is dictated by the dependency of its CSCs and not its bulk tumor cells on the selected pathway. Second, we show that it is possible to predict prior to treatment whether a tumor will acquire resistance via a genetic or epigenetic

mechanism based on the phenotype of its CSCs. Although the translation of this approach is currently challenging, it has significant clinical implications in terms of guiding second-line therapy selection or designing combination therapies in a timely manner. Third, we reveal a new mechanism of therapeutic resistance: epigenetic reprogramming of bulk tumor cells through changes in histone acetylation via enhanced degradation of specific HATs resulting in an altered histone code. A previous study reported that transformed Smo/Smo MB tissues have increased HDAC1, HDAC2, and HDAC3 and decreased HDAC11 expression compared to wild-type or untransformed Smo/Smo cerebellum tissues (46), suggesting that dysregulated histone acetylation may be integral to MB formation. Consistently, HDAC inhibitors were identified as potentially efficacious therapies for MBs in multiple drug screening studies (47,48). Here, we show that while control-treated SI-CSCs are insensitive to the HDAC inhibitor TSA, LDE225-resistant SI-CSCs are sensitive and suggest combining SMO and HDAC inhibitors for SMOi-resistant SI-CSC tumors. This study paves the way for precision medicine, including the application of targeted therapies and managing therapy resistance, especially in cases where mutations in the targeted pathway are not apparent in the resistant tumors.

The SMO inhibitors vismodegib/GDC-0449 and sonidegib/LDE225 are currently being evaluated for treating SHH MBs(8,14–16,49). A meta-analysis of clinical trials that included MBs revealed that the combined overall response rate (ORR) for both drugs was 37% for SHH MBs and 0% for non-SHH MBs (8). Interestingly, the trial with sonidegib (14 SHH and 60 non-SHH subtypes) was biased toward the adult population (11 adult and 3 pediatric patients) and showed a higher ORR (55%). The patients in the vismodegib trials were more evenly distributed (18 adult and 14 pediatric patients), and the ORR for the SHH subtype of MB was 17%. A higher ORR in an adult-biased trial is consistent with our results. We previously showed that the transformation of neuroepithelial cells in the embryonic brain (*FSmoM2;hGFAPCre*) resulted in infantile MBs that contain SI-CSCs (18), and they are inherently resistant to SMOi, which would lower the ORR. In contrast, the transformation of committed EGL progenitors postnatally (*Fsmo;Atoh1-CreER*) resulted in adult SHH MBs that contain SD-CSCs (18); these tumors are sensitive to SMOi treatment and require acquired mutations for resistance to emerge, which may explain the higher ORR in the sonidegib trial.

Previously reported mechanisms of resistance to SMOis include mutations or amplification of SHH pathway components (4,5,9,11), activation of the PIK3/AKT (10) or Ras/MAPK (50) pathways, and persistent activation of *Gli1* expression/SHH pathway signaling via upregulated BRD4 activity (40). Here, we demonstrated that acquired mutations in the SHH pathway occur only when CSCs, not bulk tumor cells, depend on SHH signaling. Unlike a previous study implying that elevated BRD4 expression mediates SMOi resistance by activating *Gli1* transcription (40), we report that JQ1 inhibition suppresses SMOi-resistant SHH MB in the absence of significant *Gli1* expression. In addition, the majority of targeted therapy resistance mechanism studies in the field rely on bulk tumor analysis. In contrast, this study emphasizes the role of epigenetic cellular heterogeneity and cell-state-specific responses to targeted therapy. It provides compelling in vivo evidence that in some tumors, CSCs and bulk tumor cells depend on different mitogenic/survival signaling pathways. A significant consequence of this critical difference is that targeted therapies selected by bulk

tumor analysis may not be effective against CSCs in some tumors. In these cases, there is no selective pressure for genetic mutations in the CSCs to the targeted pathway (Supp Fig 6). We propose that the ability to predict specific mechanisms of resistance in individual tumors will greatly enhance the personalization of rational combinations or second-line therapies for patients who acquire or show de novo resistance to targeted therapy. For example, to address resistance to SMOis in patients with BCC and MBs (4,5,13), second-line therapies inhibiting downstream activators of the SHH pathway, such as GLI, are being investigated (37,51). However, our study suggests that additional SHH pathway inhibition will be ineffective in SI-CSC-containing tumors (Fig 2C) and that patients with these tumors may be insensitive to additional SMO or SHH signaling pathway inhibitors such as GANT61 (36,37). Instead, SI-CSC tumors may be retrospectively identified by decreased histone acetylation as a biomarker (Fig 5) and treated with HDAC inhibitors or BRD2/4 inhibitors (Fig 5F, G).

In summary, this study provides a new conceptual framework to understand therapy resistance mechanisms and identifies potential biomarkers to infer whether clinical resistance to SMOis is acquired via genetically or epigenetically driven mechanisms. It will be important to test whether the epigenetic mechanism we discovered (histone acetylation regulation) plays a broader role in therapeutic resistance in other cancer types, particularly in pediatric cancers, where epigenetic mechanisms play critical roles in tumorigenesis (52,53).

Supplementary Material

Refer to Web version on PubMed Central for supplementary material.

ACKNOWLEDGMENTS

We thank Patsy Nishina, Dorothy Lewis, and Carmen Ribinett for editing and providing critical comments on the manuscript.

This study was supported by the American Brain Tumor Association Discovery Award, the Department of Defense (W81XWH-14-1-0115), the Cancer Prevention and Research Institute of Texas (CPRIT; RP180882), and The Donaldson Charitable Foundation to K. Yun. It was also supported by Donna and Kenneth Peak, The Kenneth R. Peak Foundation, The John S. Dunn Foundation, The Taub Foundation, The Blanche Green Fund of the Pauline Sterne Wolff Memorial Foundation, The Kelly Kicking Cancer Foundation, The Methodist Hospital Foundation & The Veralan Foundation to D. Baskin. It was also supported by the Jackson Laboratory Cancer Center fund (P30CA034196). JHC was funded by the National Cancer Institute award numbers P30CA034196 and R21CA191848. MGL was supported by grants from the Cancer Prevention and Research Institute of Texas (CPRIT; RP140271), the NIH (R01CA157919, R01CA207098, and R01CA207109), and the Center for Cancer Epigenetics at MD Anderson. NA was supported by the DOD Horizon Award (CA191052).

REFERENCES

1. Raleigh DR, Reiter JF. Misactivation of Hedgehog signaling causes inherited and sporadic cancers. J Clin Invest 2019;129:465–75 [PubMed: 30707108]
2. Northcott PA, Robinson GW, Kratz CP, Mabbott DJ, Pomeroy SL, Clifford SC, et al. Medulloblastoma. Nat Rev Dis Primers 2019;5:11 [PubMed: 30765705]
3. Boumahdi S, de Sauvage FJ. The great escape: tumour cell plasticity in resistance to targeted therapy. Nat Rev Drug Discov 2020;19:39–56 [PubMed: 31601994]
4. Atwood SX, Sarin KY, Whitson RJ, Li JR, Kim G, Rezaee M, et al. Smoothened variants explain the majority of drug resistance in basal cell carcinoma. Cancer cell 2015;27:342–53 [PubMed: 25759020]

5. Sharpe HJ, Pau G, Dijkgraaf GJ, Basset-Seguin N, Modrusan Z, Januario T, et al. Genomic analysis of smoothened inhibitor resistance in basal cell carcinoma. Cancer cell 2015;27:327–41 [PubMed: 25759019]
6. Chang AL, Oro AE. Initial assessment of tumor regrowth after vismodegib in advanced Basal cell carcinoma. Arch Dermatol 2012;148:1324–5 [PubMed: 22910979]
7. Wolfe CM, Green WH, Cognetta AB Jr., Hatfield HK. Basal cell carcinoma rebound after cessation of vismodegib in a nevoid basal cell carcinoma syndrome patient. Dermatol Surg 2012;38:1863–6 [PubMed: 22805146]
8. Li Y, Song Q, Day BW. Phase I and phase II sonidegib and vismodegib clinical trials for the treatment of paediatric and adult MB patients: a systemic review and meta-analysis. Acta Neuropathol Commun 2019;7:123 [PubMed: 31362788]
9. Kool M, Jones DT, Jager N, Northcott PA, Pugh TJ, Hovestadt V, et al. Genome sequencing of SHH medulloblastoma predicts genotype-related response to smoothened inhibition. Cancer cell 2014;25:393–405 [PubMed: 24651015]
10. Buonamici S, Williams J, Morrissey M, Wang A, Guo R, Vattay A, et al. Interfering with resistance to smoothened antagonists by inhibition of the PI3K pathway in medulloblastoma. Sci Transl Med 2010;2:51ra70
11. Yauch RL, Dijkgraaf GJ, Alicke B, Januario T, Ahn CP, Holcomb T, et al. Smoothened mutation confers resistance to a Hedgehog pathway inhibitor in medulloblastoma. Science 2009;326:572–4 [PubMed: 19726788]
12. Dijkgraaf GJ, Alicke B, Weinmann L, Januario T, West K, Modrusan Z, et al. Small molecule inhibition of GDC-0449 refractory smoothened mutants and downstream mechanisms of drug resistance. Cancer research 2011;71:435–44 [PubMed: 21123452]
13. Rudin CM, Hann CL, Laterra J, Yauch RL, Callahan CA, Fu L, et al. Treatment of medulloblastoma with hedgehog pathway inhibitor GDC-0449. The New England journal of medicine 2009;361:1173–8 [PubMed: 19726761]
14. LoRusso PM, Rudin CM, Reddy JC, Tibes R, Weiss GJ, Borad MJ, et al. Phase I trial of hedgehog pathway inhibitor vismodegib (GDC-0449) in patients with refractory, locally advanced or metastatic solid tumors. Clin Cancer Res 2011;17:2502–11 [PubMed: 21300762]
15. Gajjar A, Stewart CF, Ellison DW, Kaste S, Kun LE, Packer RJ, et al. Phase I study of vismodegib in children with recurrent or refractory medulloblastoma: a pediatric brain tumor consortium study. Clin Cancer Res 2013;19:6305–12 [PubMed: 24077351]
16. Robinson GW, Orr BA, Wu G, Gururangan S, Lin T, Qaddoumi I, et al. Vismodegib Exerts Targeted Efficacy Against Recurrent Sonic Hedgehog-Subgroup Medulloblastoma: Results From Phase II Pediatric Brain Tumor Consortium Studies PBTC-025B and PBTC-032. Journal of clinical oncology : official journal of the American Society of Clinical Oncology 2015;33:2646–54 [PubMed: 26169613]
17. Marino S. Medulloblastoma: developmental mechanisms out of control. Trends Mol Med 2005;11:17–22 [PubMed: 15649818]
18. Chow KH, Shin DM, Jenkins MH, Miller EE, Shih DJ, Choi S, et al. Epigenetic states of cells of origin and tumor evolution drive tumor-initiating cell phenotype and tumor heterogeneity. Cancer research 2014;74:4864–74 [PubMed: 25136069]
19. Yang ZJ, Ellis T, Markant SL, Read TA, Kessler JD, Bourboulas M, et al. Medulloblastoma can be initiated by deletion of Patched in lineage-restricted progenitors or stem cells. Cancer cell 2008;14:135–45 [PubMed: 18691548]
20. Ahlfeld J, Favaro R, Pagella P, Kretzschmar HA, Nicolis S, Schuller U. Sox2 requirement in sonic hedgehog-associated medulloblastoma. Cancer research 2013;73:3796–807 [PubMed: 23596255]
21. Vanner RJ, Remke M, Gallo M, Selvadurai HJ, Coutinho F, Lee L, et al. Quiescent sox2(+) cells drive hierarchical growth and relapse in sonic hedgehog subgroup medulloblastoma. Cancer cell 2014;26:33–47 [PubMed: 24954133]
22. Chen J, Li Y, Yu T-S, McKay RM, Burns DK, Kernie SG, et al. A restricted cell population propagates glioblastoma growth after chemotherapy. Nature 2012;488:522–6 [PubMed: 22854781]

23. Bao S, Wu Q, McLendon RE, Hao Y, Shi Q, Hjelmeland AB, et al. Glioma stem cells promote radioresistance by preferential activation of the DNA damage response. Nature 2006;444:756–60 [PubMed: 17051156]
24. Visvader JE, Lindeman GJ. Cancer stem cells: current status and evolving complexities. Cell Stem Cell 2012;10:717–28 [PubMed: 22704512]
25. Lathia JD, Mack SC, Mulkearns-Hubert EE, Valentim CL, Rich JN. Cancer stem cells in glioblastoma. Genes Dev 2015;29:1203–17 [PubMed: 26109046]
26. Alcantara Llaguno S, Chen J, Kwon CH, Jackson EL, Li Y, Burns DK, et al. Malignant astrocytomas originate from neural stem/progenitor cells in a somatic tumor suppressor mouse model. Cancer cell 2009;15:45–56 [PubMed: 19111880]
27. McKenna A, Hanna M, Banks E, Sivachenko A, Cibulskis K, Kernytsky A, et al. The Genome Analysis Toolkit: a MapReduce framework for analyzing next-generation DNA sequencing data. Genome research 2010;20:1297–303 [PubMed: 20644199]
28. Cingolani P, Platts A, Wang le L, Coon M, Nguyen T, Wang L, et al. A program for annotating and predicting the effects of single nucleotide polymorphisms, SnpEff: SNPs in the genome of Drosophila melanogaster strain w1118; iso-2; iso-3. Fly (Austin) 2012;6:80–92 [PubMed: 22728672]
29. Jung SY, Choi JM, Rousseaux MW, Malovannaya A, Kim JJ, Kutzera J, et al. An Anatomically Resolved Mouse Brain Proteome Reveals Parkinson Disease-relevant Pathways. Mol Cell Proteomics 2017;16:581–93 [PubMed: 28153913]
30. Krueger F, Andrews SR. Bismark: a flexible aligner and methylation caller for Bisulfite-Seq applications. Bioinformatics 2011;27:1571–2 [PubMed: 21493656]
31. Langmead B, Salzberg SL. Fast gapped-read alignment with Bowtie 2. Nat Methods 2012;9:357–9 [PubMed: 22388286]
32. Akalin A, Kormaksson M, Li S, Garrett-Bakelman FE, Figueroa ME, Melnick A, et al. methylKit: a comprehensive R package for the analysis of genome-wide DNA methylation profiles. Genome Biol 2012;13:R87 [PubMed: 23034086]
33. Cavalli FMG, Remke M, Rampasek L, Peacock J, Shih DJH, Luu B, et al. Intertumoral Heterogeneity within Medulloblastoma Subgroups. Cancer cell 2017;31:737–54 e6 [PubMed: 28609654]
34. Mao J, Ligon KL, Rakhlin EY, Thayer SP, Bronson RT, Rowitch D, et al. A novel somatic mouse model to survey tumorigenic potential applied to the Hedgehog pathway. Cancer research 2006;66:10171–8 [PubMed: 17047082]
35. Schuller U, Heine VM, Mao J, Kho AT, Dillon AK, Han YG, et al. Acquisition of granule neuron precursor identity is a critical determinant of progenitor cell competence to form Shh-induced medulloblastoma. Cancer cell 2008;14:123–34 [PubMed: 18691547]
36. Lauth M, Bergstrom A, Shimokawa T, Toftgard R. Inhibition of GLI-mediated transcription and tumor cell growth by small-molecule antagonists. Proc Natl Acad Sci U S A 2007;104:8455–60 [PubMed: 17494766]
37. Dong X, Wang C, Chen Z, Zhao W. Overcoming the resistance mechanisms of Smoothened inhibitors. Drug Discov Today 2018;23:704–10 [PubMed: 29326074]
38. Brown R, Curry E, Magnani L, Wilhelm-Benartzi CS, Borley J. Poised epigenetic states and acquired drug resistance in cancer. Nat Rev Cancer 2014;14:747–53 [PubMed: 25253389]
39. Yang C, Zhang J, Ma Y, Wu C, Cui W, Wang L. Histone methyltransferase and drug resistance in cancers. J Exp Clin Cancer Res 2020;39:173
40. Tang Y, Gholamin S, Schubert S, Willardson MI, Lee A, Bandopadhayay P, et al. Epigenetic targeting of Hedgehog pathway transcriptional output through BET bromodomain inhibition. Nature medicine 2014;20:732–40
41. Verreault A, Kaufman PD, Kobayashi R, Stillman B. Nucleosomal DNA regulates the core-histone-binding subunit of the human Hat1 acetyltransferase. Curr Biol 1998;8:96–108 [PubMed: 9427644]
42. Jin Q, Yu LR, Wang L, Zhang Z, Kasper LH, Lee JE, et al. Distinct roles of GCN5/PCAF-mediated H3K9ac and CBP/p300-mediated H3K18/27ac in nuclear receptor transactivation. EMBO J 2011;30:249–62 [PubMed: 21131905]

43. Das C, Lucia MS, Hansen KC, Tyler JK. CBP/p300-mediated acetylation of histone H3 on lysine 56. Nature 2009;459:113–7 [PubMed: 19270680]
44. Bolin S, Borgenvik A, Persson CU, Sundstrom A, Qi J, Bradner JE, et al. Combined BET bromodomain and CDK2 inhibition in MYC-driven medulloblastoma. Oncogene 2018;37:2850–62 [PubMed: 29511348]
45. Bandopadhayay P, Bergthold G, Nguyen B, Schubert S, Gholamin S, Tang Y, et al. BET bromodomain inhibition of MYC-amplified medulloblastoma. Clin Cancer Res 2014;20:912–25 [PubMed: 24297863]
46. Lee SJ, Lindsey S, Graves B, Yoo S, Olson JM, Langhans SA. Sonic hedgehog-induced histone deacetylase activation is required for cerebellar granule precursor hyperplasia in medulloblastoma. PLoS One 2013;8:e71455
47. Pak E, MacKenzie EL, Zhao X, Pazyra-Murphy MF, Park PMC, Wu L, et al. A large-scale drug screen identifies selective inhibitors of class I HDACs as a potential therapeutic option for SHH medulloblastoma. Neuro Oncol 2019;21:1150–63 [PubMed: 31111916]
48. Pei Y, Liu KW, Wang J, Garancher A, Tao R, Esparza LA, et al. HDAC and PI3K Antagonists Cooperate to Inhibit Growth of MYC-Driven Medulloblastoma. Cancer cell 2016;29:311–23 [PubMed: 26977882]
49. Kieran MW, Chisholm J, Casanova M, Brandes AA, Aerts I, Bouffet E, et al. Phase I study of oral sonidegib (LDE225) in pediatric brain and solid tumors and a phase II study in children and adults with relapsed medulloblastoma. Neuro Oncol 2017;19:1542–52 [PubMed: 28605510]
50. Zhao X, Ponomaryov T, Ornell KJ, Zhou P, Dabral SK, Pak E, et al. RAS/MAPK Activation Drives Resistance to Smo Inhibition, Metastasis, and Tumor Evolution in Shh Pathway-Dependent Tumors. Cancer research 2015;75:3623–35 [PubMed: 26130651]
51. Didiasova M, Schaefer L, Wygrecka M. Targeting GLI Transcription Factors in Cancer. Molecules 2018;23
52. Jones DTW, Banito A, Grunewald TGP, Haber M, Jager N, Kool M, et al. Molecular characteristics and therapeutic vulnerabilities across paediatric solid tumours. Nat Rev Cancer 2019;19:420–38 [PubMed: 31300807]
53. Roussel MF, Stripay JL. Epigenetic Drivers in Pediatric Medulloblastoma. Cerebellum 2018;17:28–36 [PubMed: 29178021]

SIGNIFICANCE STATEMENT

The mechanism by which individual tumors become resistant to targeted therapies is thought to be unpredictable. This study provides novel insights into how selective pressure on cancer stem vs. bulk tumor cells drives distinct and predictable mechanisms of resistance to targeted therapies. This finding paves a way for future treatment strategies that incorporate anticipated resistance mechanisms in devising second-line therapies in a personalized manner.

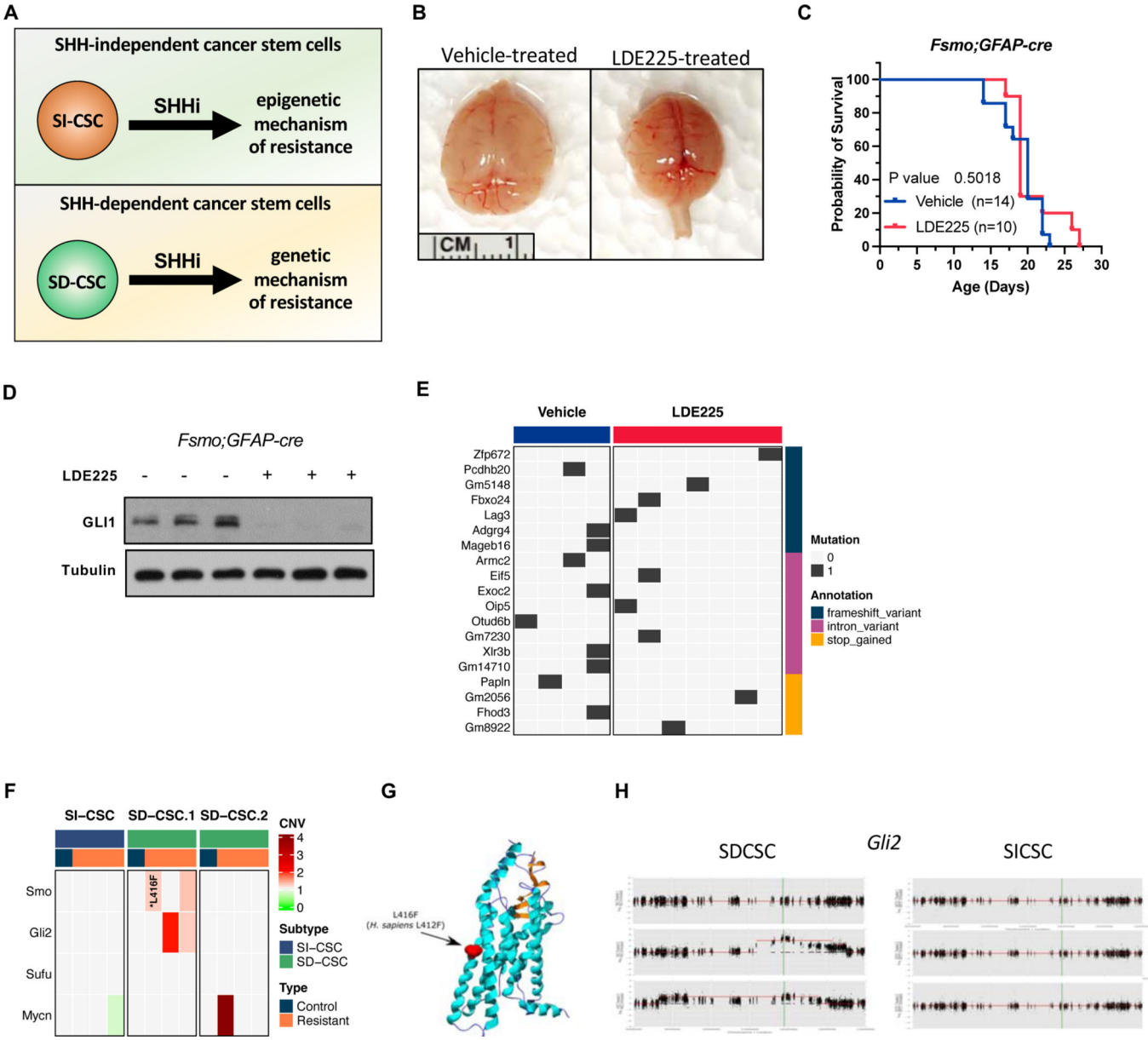

Figure 1. SMOi-induced mutations to SHH pathway genes only occur in MBs in which CSCs depend on the SHH signaling.

A) A schematic of the major hypothesis tested in the study. **B**) Gross images of vehicle and LDE225-treated *fSmoM2;hGFAP-cre* brains at harvest. **C**) Kaplan-Meier survival curve analysis showing no significant survival benefit of LDE225 treatment. **D**) GLI1 protein level is reduced in LDE-treated *fSmoM2;GFAPcre* tumors in vivo. **E**) A summary of high impact mutations in vehicle and LDE225 treated *fSmoM2;hGFAP-cre* MBs. **F)** A summary of identified mutations and copy number alterations in SHH pathway genes in SMOi-resistant SI-CSC and SD-CSC *Ptch;p53* MB. **G)** LDE225-induced *SMO* mutation in *Ptch;p53* SD-CSC tumor. **H)** LDE225-induced *Gli2* amplification observed in two SD-CSC tumors from the same cohort, which is not observed in any SI-CSC MBs. CNV compared to Vehicle treated tumor from the same cohort.

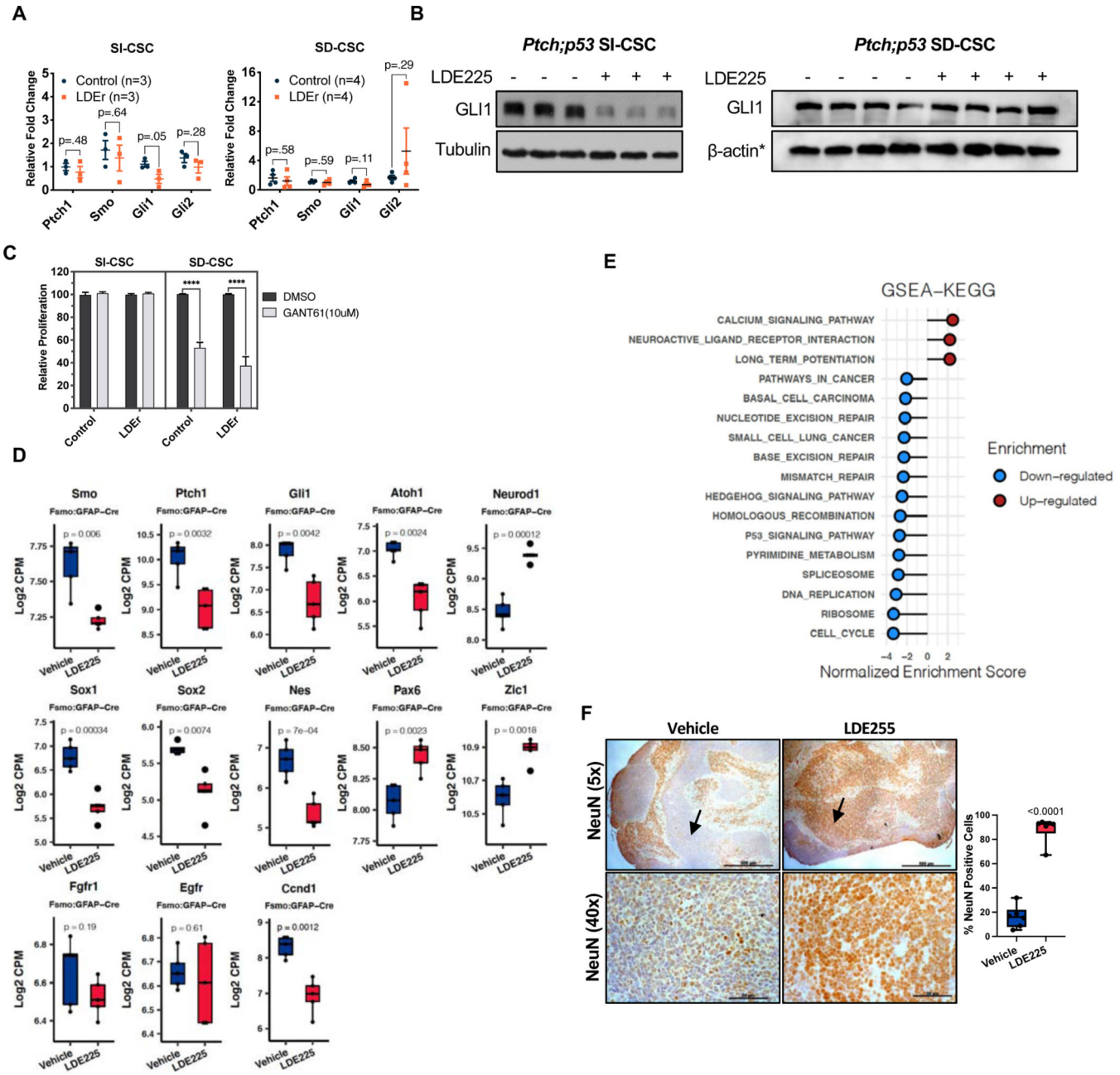

Figure 2. SMOi-resistant SI-CSC MBs grow independently of the SHH pathway.

A) Realtime RT-PCR analyses of SHH pathway genes in *Ptch;p53* SI-CSC and SD-CSC MBs treated with vehicle or LDE225 tumors. Error bars represent SEM. P-values were calculated using two-tailed Student's t-test. **B)** GLI1 protein levels in control and LDE225-resistant *Ptch;p53* SI-CSC and SD-CSC tumors. *ß-ACTIN loading control is the same as shown in Figures 4C and F as the same blot was stripped and probed with multiple antibodies due to limited sample amounts. **C)** GANT61 (GLI inhibitor) treatment of *Ptch;p53* SI-CSC and SD-CSC tumorsphere cells in vitro. N=3, ****P < 0.0001, by two-tailed Student's t-test. Error bars represent SEM. **D)** RNA-seq expression levels of *SHH,* neuronal stem cell and differentiation markers in vehicle vs. LDE225-treated

fSmoM2;GFAP-cre MBs. Box represents log_2-scaled CPM range in RNA-seq data. Central line represents the mean. P-values were calculated using two-tailed Student's t-test. **E)** GSEA analyses (2<NES >2)of *fSmoM2;hGFAP-cre* SI-CSC tumors showing negative enrichment of the hedgehog signaling pathway, cell cycle, DNA-repair and other gene sets and positive enrichment for gene sets associated with neuronal differentiation and function in LDE225-resistant SI-CSC tumors. **F)** Representative immunohistochemistry images showing increased NEUN expressing cells in LDE225-treated *fSmoM2M2;hGFAPcre* MBs. Low magnification shows overall increase in NEUN positive cells throughout the LDE-treated cerebellum. High magnification images taken from high cellular density areas. Six representative fields from 3 matched pairs of vehicle vs. LDE treated samples were counted manually. Scale bar (5x = 500μM, 40x = 50μM). Arrows point to equivalent tumor areas with high nuclear density.

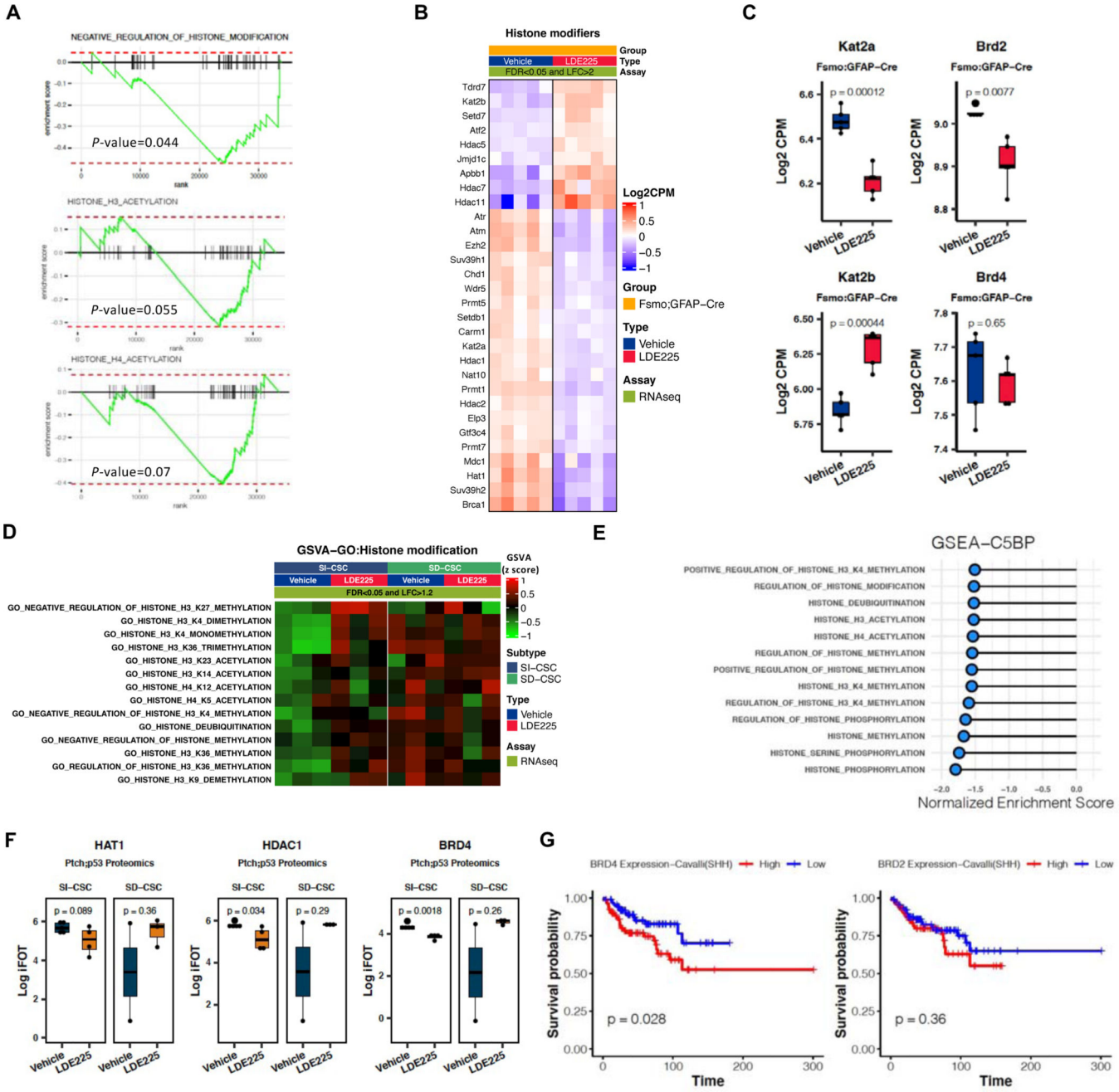

Figure 3. Unbiased RNAseq and proteomics analyses indicate altered histone modification pathways in SMOi-resistant tumors.

A) GSEA analyses showing negative enrichment of histone modification gene sets in LDE225-resistant *fSmoM2;hGFAP-cre* SI-CSC MBs. **B)** heatmap showing top DE histone modification-related genes in *fSmoM2;hGFAP-cre* MBs. FDR <0.05 and log fold change>2. Expression values were normalized and centered. **C)** Expression levels of *Kat2a, Kat2b, Brd2 and Brd4* in vehicle vs. LDE225 -treated *fSmoM2;hGFAP-cre* MBs. Box represents $\log_2$-scaled CPM range in RNA-seq data. Central line represents the mean. P-values were calculated using two-tailed Student's t-test. **D)** GSVA analyses (GSVA enrichment score

FC>1.2 and FDR<0.05) showing enrichment of histone modification gene sets in LDE225-resistant SI-CSC *Ptch;p53* but not LDE225-resistant SD-CSC *Ptch;p53* tumors. **E)** GSEA analyses (NES>1.5) of proteomics data showing negative enrichment of histone modification gene sets in LDE225-resistant *Ptch;p53* SI-CSC MBs. **F)** Expression levels of HAT1, HDAC1 and BRD4 in vehicle vs. LDE225 -treated *Ptch;p53* SI-CSC and SD-CSC tumors. Box represents log_2-scaled iFOT range in proteomics data. Central line represents the mean. P-values were calculated using two-tailed Student's t-test. **G)** Kaplan-Meier survival curves from analyzing a human medulloblastoma dataset (GSE85217, Cavalli et al., ref(33)) for SHH MB patients expressing high or low levels of *BRD2* and *BRD4*, using median cutoff. Data represent Log2 signal. P-values were calculated using ordinary one-way ANOVA with Tukey's multiple comparisons test. SHH subgroup: n = 223.

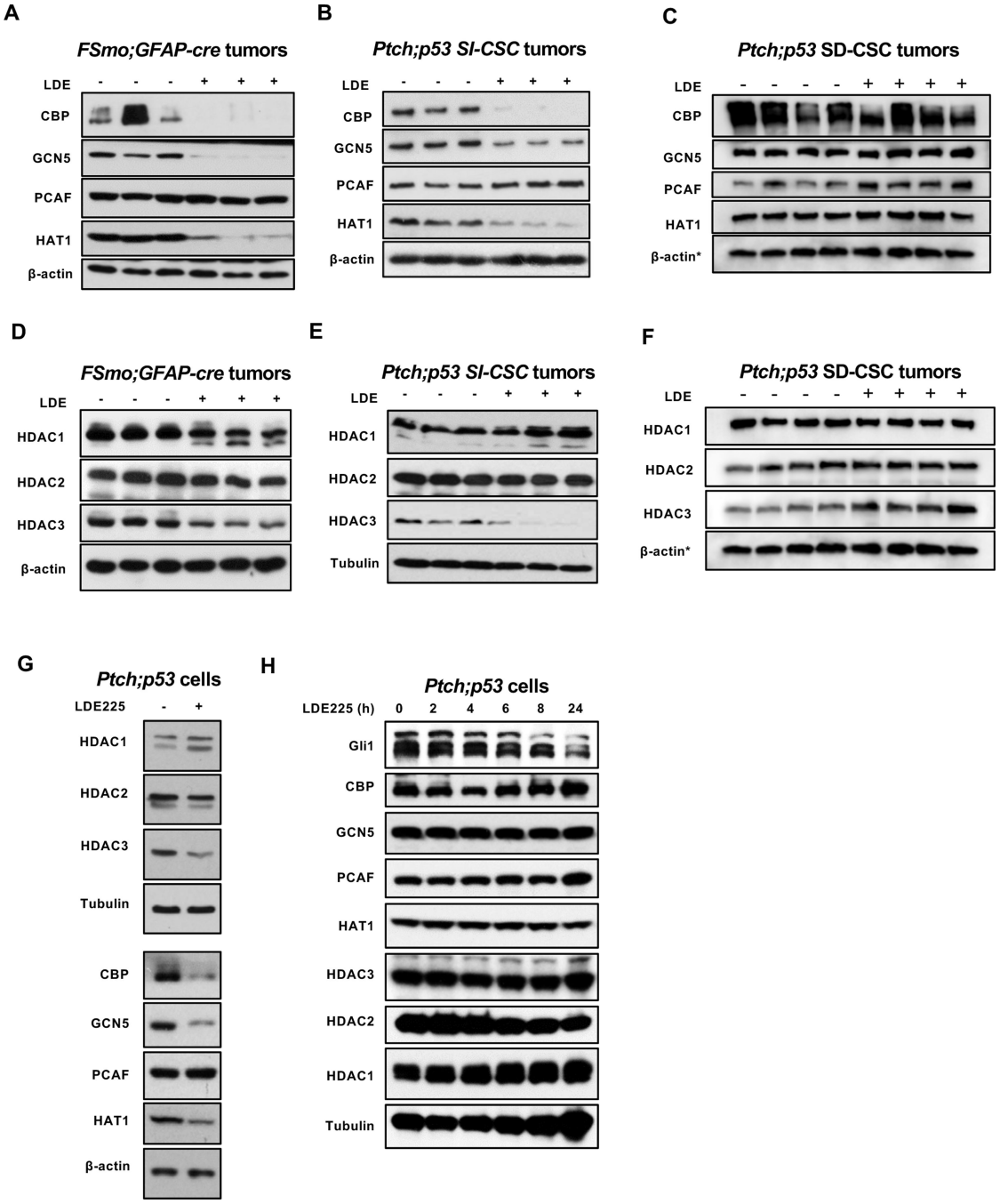

Figure 4. Chronic SMOi treatment reduces specific HAT and HDAC protein levels in SI-CSC MBs in vitro and in vivo.

Western blot analyses of histone acetyl transferases and histone deacetylases in vehicle vs. LDE225 -resistant *fSmoM2M2;hGFAP-cre* and *Ptch;p53* SHH MBs. **(A, D)** *fSmoM2M2;hGFAP-cre SI-CSC*, **(B, E)** *Ptch;p53* SI-CSC MBs and **(C, F)** *Ptch;p53* SD-CSC MBs. **G)** Western blot analyses of LDE225-resistant *Ptch;p53* SI-CSC tumorsphere cells treated with LDE225 for long-term (> 2 weeks) *in vitro* show the same HAT and HDAC expression changes. **H**) Acute (24 hours) treatment of *Ptch;p53* SI-CSC tumorsphere

cells show no significant changes in CBP, GCN5, or HAT1 protein levels in response to short-term LDE225 treatment.

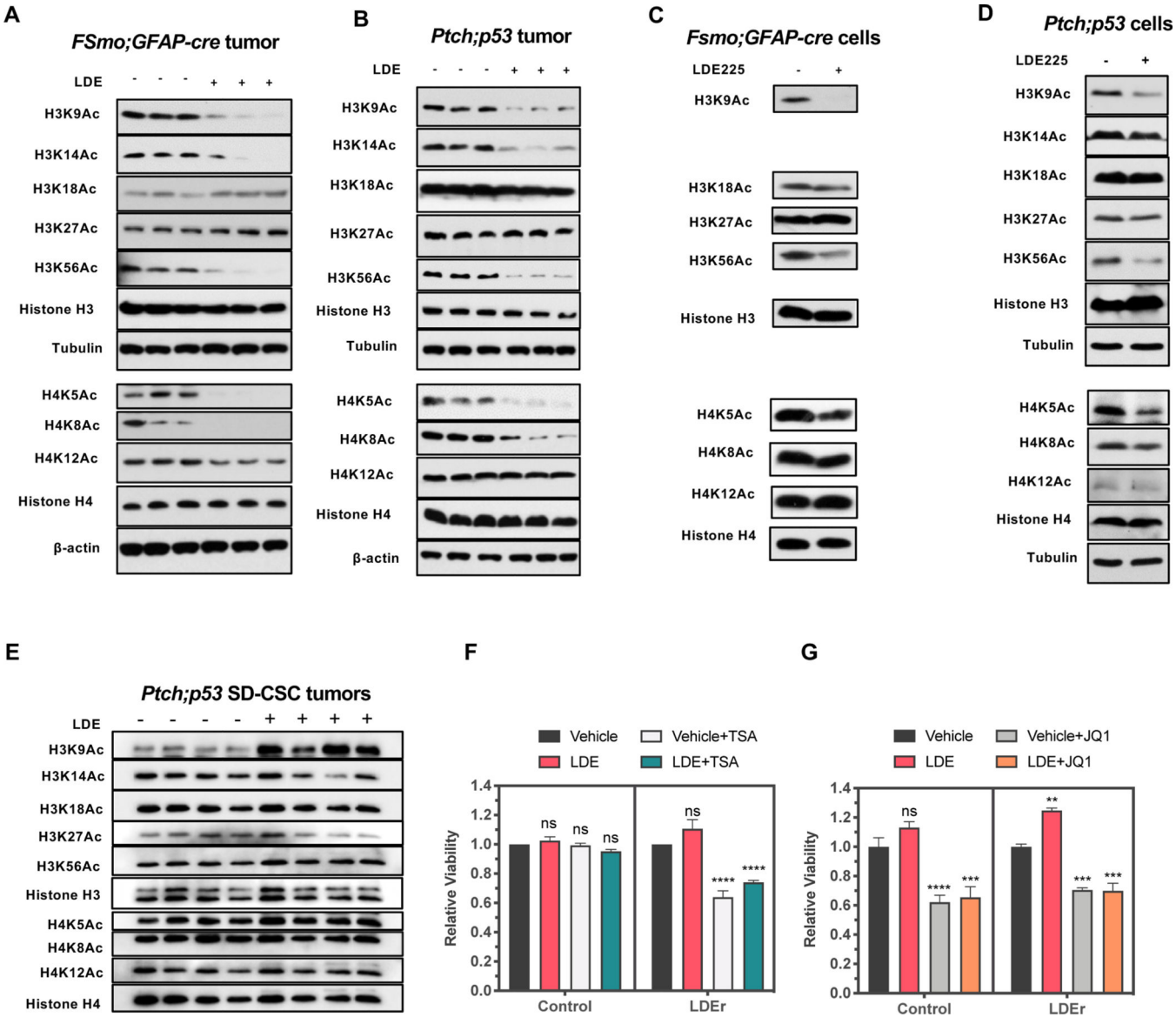

Figure 5. Decreased H3K9, H3K14, H3K56, H4K5, and H3K8 marks in SMOi-resistant SI-CSC MBs.

A, B) Western blot analyses of different histone acetylation marks comparing vehicle vs. LDE225 treated *fSmoM2;hGFAP-cre* and *Ptch;p53* MBs in vivo. **C, D)** Western blot analyses of SMOi-resistant SI-CSC tumorsphere cells from *fSmoM2;hGFAP-cre* and *Ptch;p53* MB treated with LDE225 for long-term (> 2 weeks) *in vitro* show the same HAT and histone acetylation mark changes. **E)** Western blot analyses of different histone acetylation marks comparing vehicle vs. LDE225 treated *Ptch;p53* SD-CSC MB in vivo. **F**) Epigenetically reprogrammed LDE225-resistant SI-CSCs, but not vehicle treated, are sensitive to TSA (10nM) treatment. **G**) Both control and LDE-resistant SI-CSCs are sensitive to 100nM JQ1 treatment *in vitro.* P-values were calculated using ordinary one-way ANOVA with Sidak's multiple comparisons test. N=3, ****P < 0.0001, *P < 0.05.

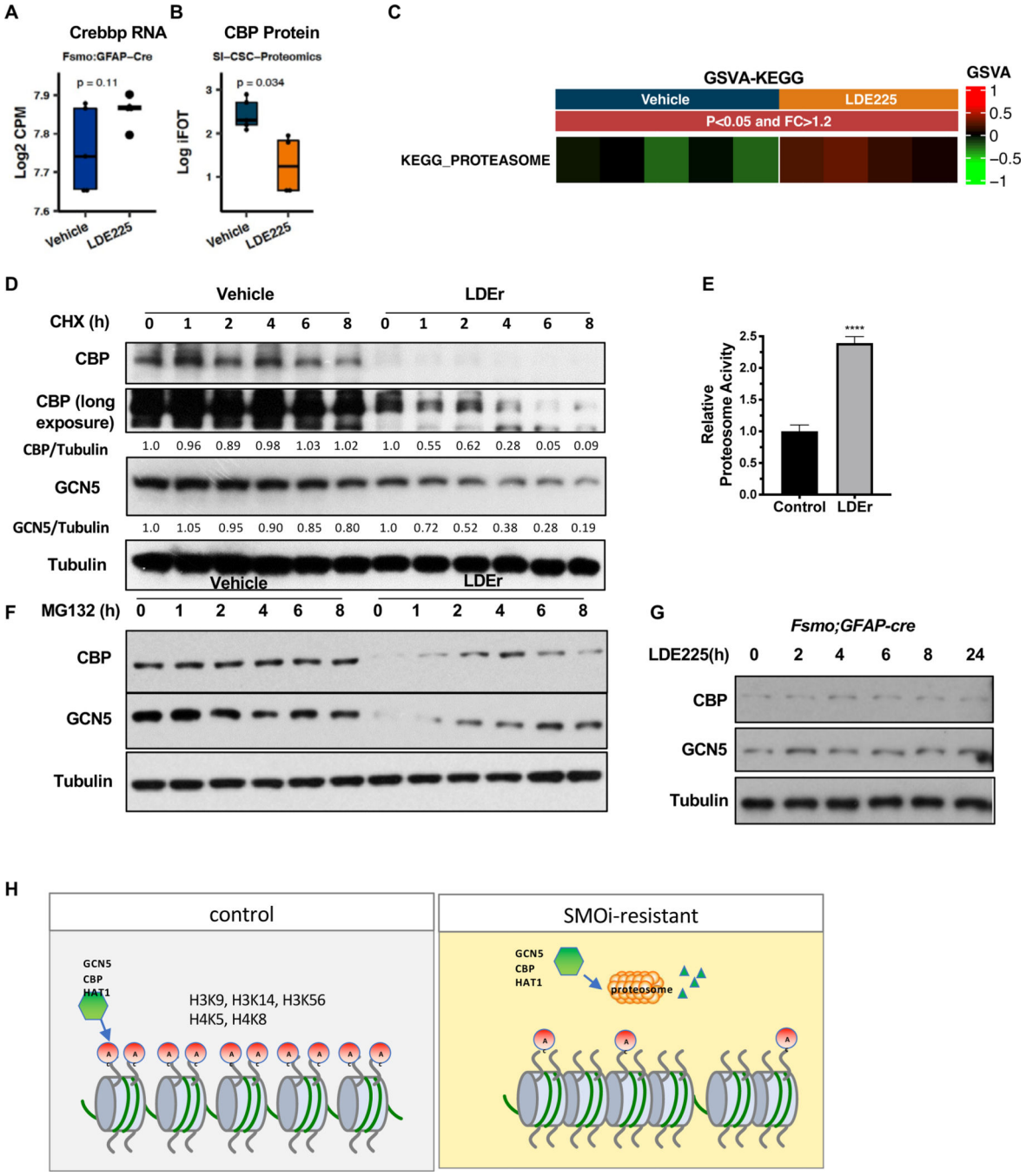

Figure 6. Increased proteasome activity in SMOi-resistant SI-CSC tumors degrade GCN5 and CBP.

A, B) Histone acetyltransferase *Crebbp*/CBP level is not altered at the RNA level (A) but is significantly reduced at the protein level (B). Also see Fig 4 A & B. **C**) Significant enrichment of the Proteasome pathway geneset in proteomics dataset in *Ptch;p53* SMOi-resistant SI-CSC MB. **D**) LDE-resistant SI-CSC cells treated with cycloheximide (CHX) show shortened half-life of CBP and GCN5 proteins compared to control. **E**) Proteasome-Glo Assay shows increased proteasomal activity in LDE-resistant SI-CSC cells. N=6, ***P

< 0.0001, by two-tailed Student's t-test. **F**) Treatment with a proteasome inhibitor, MG132, shows significant recovery of CBP and GCN5 protein levels in LDE-resistant SI-CSC cells. **G**) CBP and GCN5 protein levels are unchanged in response to acute (24 hrs) LDE treatment in *fSmoM2;hGFAPcre* tumorsphere cells in vitro. **H**) A working model of epigenetically reprogrammed therapy resistance in SI-CSCs MBs.